Trans. JSASS Aerospace Tech. Japan
Vol. 19, No. 5, pp. 639-646, 2021
DOI: 10.2322/tastj.19.639

DEM Analysis and Evaluation of Hopping Motion on a Sandy Surface in Microgravity

By Keita KOBASHI,[1)] Kenji NAGAOKA,[2)] and Kazuya YOSHIDA[1)]

[1)]*Department of Aerospace Engineering, Tohoku University, Sendai, Japan*
[2)]*Department of Mechanical and Control Engineering, Kyushu Institute of Technology, Kitakyushu, Japan*

(Received July 12th, 2019)

Hopping mobility is effective for exploration robots present on small celestial bodies including asteroids and comets and their surfaces are covered in certain places with granular materials such as fine grain sand. However, existing studies do not address hopping mobility on the aforementioned types of granular materials in detail. Therefore, it is necessary to analyze hopping motion on sandy surface for future missions. This study presents a parametric analysis of the hopping motion on granular materials based on a discrete element method (DEM) simulation. In particular, the DEM allows for the numerical simulation of the dynamic behaviors of numerous fine particles. The DEM defines a sand particle as a simple sphere and computes mechanical interaction between each particle which follows some simple laws of dynamics. To analyze the hopping motion, we focus on two characteristics of the hopping motion: the initial hop velocity and hop angle of the robot. In DEM simulations, we change the friction and rolling friction coefficient of the sand particles, the acceleration of gravity and the angular velocity of the robot. We perform a simplified analysis and assume that the terrain surface in DEM simulation is smooth and flat and that the robot exhibits a cubic shape. Based on the research results, we qualitatively evaluate the exploration robot's motion on a sandy surface by DEM analysis when compared with its motion on a rigid surface.

Key Words: Asteroid Exploration, Sandy Surface, Hopping Robot, DEM, Parametric Analysis

1. Introduction

The exploration of asteroids to clarify their composition is a mission that is actively planned and executed by countries recently given its significance in revealing information on the origin of the solar system.[1,2)] Therefore, it is important to explore asteroids via probes and robots that can move on the actual surface of asteroids.

In 2005, Hayabusa,[3,4)] an asteroid explorer developed by the Japan Aerospace Exploration Agency (JAXA), succeeded in its mission of collecting a sample from an asteroid called "Itokawa". Exploration on asteroid surface is required to obtain more information regarding asteroids. Generally, exploration robots that can traverse an asteroid surface play a crucial role in asteroid surface exploration.

The characteristics of the environment on asteroids include the existence of microgravity (the average of magnitude lies between $10^{-5}\mathrm{m/s^2}$ and $10^{-3}\mathrm{m/s^2}$) and uneven surfaces. On asteroid surfaces, the frictional force that acts on a robot is extremely low due to the microgravity environment of asteroids in the case when exploration robots do not actively push the surface and a robot can easily leave the asteroid surface by reaction forces. National Aeronautics and Space Administration Jet Propulsion Laboratory (NASA/JPL) once launched a project to explore the asteroid surface and developed a tiny rover named MUSES CN[5)] that adopts wheeled mobility. The robots that adopt wheeled mobility are highly affected by the reaction force which accompanies the rotation of the wheels and contacts between wheels and asteroid surfaces. Hence, the robots are unable to move fast and do not exhibit time efficiency of traveling. The MUSES CN rover did not overcome the problem of developed cost, which was due to microgravity, and the project was aborted.

An example of asteroid exploring robots includes MINERVA,[6)] which was developed by JAXA, MASCOT[7)] developed by German Aerospace Center (DLR), National Center of Space Studies (CNES) and JAXA and Hedgehog[8)] developed by Stanford University and NASA/JPL. All the aforementioned examples adopted the use of hopping mobility. The hopping mobility is generated by reaction torque from the internal mechanism of the robot. Robots use hopping mobility to actively push the surface of the ground. Thus, a high frictional force acts on a robot even if the robot is in a microgravity environment. Therefore, robots can obtain high horizontal velocity while hopping on asteroid surfaces. The hopping mobility allows for a high performance in leaping over obstacles and high travelling time efficiency. Furthermore, the three robots exhibit the advantage of a simplified structure in which their actuator is enclosed inside their bodies. Hence, the hopping movement is an appropriate moving method for this application. The feasibility of hopping motion on rigid surfaces was validated by experiments.[6,8)]

In the real case, asteroid surfaces are covered in certain places with granular materials such as fine grain sand.[9)] The motion of wheeled mobility on a lunar regolith and motion of dynamic anchors (which are attached to the feet of landers on a granular surface) are analyzed via simulation.[10,11)] However, the feasibility of that motion on sandy surface is not analyzed in detail.

In the study, an analysis of the characteristics of the hopping mobility on sandy surface is performed via numerical simulations. In the numerical simulation, the discrete element method (DEM) was used.[12)] Specifically, DEM calculates the interaction between particles that are represented by a simple sphere based on simple dynamics model and simulates the complete

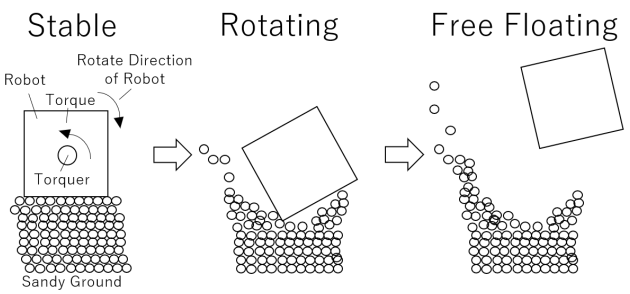

Fig. 1. Hopping sequence.

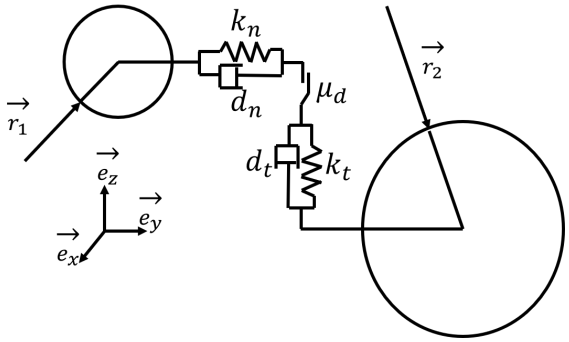

Fig. 2. Contact model of DEM.

complex motion of a few granular materials. Therefore, the use of DEM makes it is easy to analyze the motions of sand particles parametrically.

We focus on the hop angle and initial translational velocity of the robot and analyze hopping motion via altering the friction coefficient, rolling friction coefficient of sand particles, acceleration of gravity, and torque of the torquer. Following the analysis, we qualitatively evaluate the hopping motions. Furthermore, to evaluate the hopping motion on sandy surface relatively, we compare the hopping motion on a sandy surface with similar motion on a rigid surface and discuss the characteristics of the motion of the robot on a sandy surface by focussing on hop angle and initial hop velocity of the robot.

The study consists of the following structure. Section 2 discusses the hopping mechanism. Section 3 presents the dynamics model of DEM. Section 4 describes the numerical simulations of the hopping motion and effects of changing parameters. Section 5 presents a comparison of the hopping motion on a rigid surface and granular surface.

2. Hopping Motion

In this study, we set the following two preconditions.

1. The rover should cover whole asteroid surfaces.
2. Granular materials which are dealt in this study do not have cohesion.

Given microgravity, an exploration robot using wheeled mobility experiences considerably low friction force for locomotion, and thus the mobility provides the robot with extremely low velocity. Hence, typical wheeled mobility is inefficient to investigate whole asteroid surfaces. To solve the problem, an asteroid exploration robot adopts hopping mobility via reaction torque that is generated by an internal built-in torquer. In the study, hopping refers to the reaction torque applied by the robot torquer when it actively pushes the ground and the robot is pushed up by the reaction force. The internal torquer of the robot rotates, and the robot receives a reaction torque. Subsequently, the robot rotates by its reaction torque, and it pushes the ground. Finally, the robot receives reaction force from the ground and hops. The sequence is shown in Fig. 1. In the study, we assume that the shape of exploration robot is cubic, and it exhibits an internal torquer that is located at the geometric center of the cube (see Fig. 1).

3. Dynamics Model of DEM

DEM is a method to calculate the behavior of particles and interactions between them. It computes the movement of each particle for each time step and simulates up to millions of particles by combining the results of the calculations.

The dynamics model of DEM is shown in Fig. 2. Specifically, DEM defines a sand particle as a simple sphere and calculates the mechanical interaction between particles by using springs and dampers. The reaction force is given by Eq. (1) – Eq. (3).

$$\begin{cases} F_n = k_n \delta_{n_{ij}} - d_n v_{n_{ij}} \\ F_t = k_t \delta_{t_{ij}} - d_t v_{t_{ij}} \end{cases} \tag{1}$$

$$F = F_n + F_t \tag{2}$$

$$F_t \leqq \mu_d F_n \tag{3}$$

In particular, k_n and k_t denote normal and tangential elastic coefficients, respectively, of a linear spring. Additionally, d_n and d_t denote vertical and shear damping coefficients, respectively, of a damper. Furthermore, δn_{ij} and δt_{ij} denote normal and tangential penetrations, respectively, of two particles, and vn_{ij} and vt_{ij} denote normal and tangential relative velocities, respectively, of two particles. Moreover, μ_d denotes the dynamic friction coefficient.

In the study, we use the Hertzian model to compute the interaction of particles.[13,14] Therefore, the coefficients in the former equations are given by the following equations:

$$k_n = \frac{4}{3} E^* \sqrt{R^* \delta_n} \tag{4}$$

$$d_n = -2 \sqrt{\frac{5}{6}} \beta \sqrt{S_n m^*} \tag{5}$$

$$k_t = 8 G^* \sqrt{R^* \delta_n} \tag{6}$$

$$d_t = -2 \sqrt{\frac{5}{6}} \beta \sqrt{S_t m^*} \tag{7}$$

$$S_n = 2 E^* \sqrt{R^* \delta_n} \tag{8}$$

$$S_t = 8 G^* \sqrt{R^* \delta_n} \tag{9}$$

$$\beta = \frac{\ln(e)}{\sqrt{\ln(e) + \pi^2}} \tag{10}$$

$$\frac{1}{E^*} = \frac{1 - {\nu_1}^2}{E_1} + \frac{1 - {\nu_2}^2}{E_2} \tag{11}$$

$$\frac{1}{G^*} = \frac{2(2 - \nu_1)(1 + \nu_1)}{E_1} + \frac{2(2 - \nu_2)(1 + \nu_2)}{E_2} \tag{12}$$

$$\frac{1}{R^*} = \frac{1}{R_1} + \frac{1}{R_2} \tag{13}$$

$$\frac{1}{m^*} = \frac{1}{m_1} + \frac{1}{m_2} \tag{14}$$

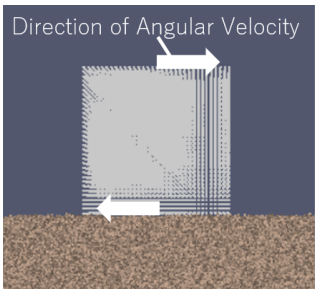

Fig. 3. Applying torque in DEM.

In particular, E denotes Young's modulus, G denotes shear modulus, ν denotes Poisson ' s ratio, and e denotes the coefficient of restitution.

Moreover, the dynamics model of rolling friction in DEM is elastic-plastic spring-dashpot (EPSD) model.[15] In this model, the rolling friction is given by the following equations:

$$k_r = 2.25 k_n \mu_r^2 R^{*2} \tag{15}$$

$$\Delta {M_r}^k = -k_r \Delta \theta_r \tag{16}$$

$${M_{r,t+\Delta t}}^k = {M_{r,t}}^k + \Delta {M_r}^k \tag{17}$$

$$|{M_{r,t+\Delta t}}^k| \leq {M_r}^m \tag{18}$$

$${M_r}^m = \mu_r R^* F_n \tag{19}$$

In Particular, k_r denotes the rolling stiffness depending on the normal elastic coefficient, the rolling friction coefficient (μ_r) and the effective radius (R^*). $\Delta\theta_r$ denotes the incremental relative rotation between particles and ${M_r}^m$ denotes the full mobilization torque determined by the normal force F_n and μ_r. Additionally, DEM computes the motion of particles as per the following routine:

1. Initialization of particles
2. Detect if collision occurs
3. Determine Net Force, $F_{net} = \Sigma F$
4. Determine Acceleration, $F_{net} = ma$
5. Compute new states

During the simulation, DEM repeats the steps from 2 to 5 until the end of the simulation.

4. Numerical Simulation

A numerical simulation of hopping motion was executed by using LIGGGHTS, a solver for DEM. In the DEM simulation, the robot is represented by an assembly of particles. To apply reaction torque to the robot in the DEM simulation, the particles that are located at the top and bottom of the robot are given a certain angular velocity (as shown in Fig. 3). In this section, we analyze the hopping motion on a sandy surface by focusing on its initial velocity and hop angle. An example of the DEM simulation is shown in Fig. 4. In the study, the robot rotates around an axis. Hence, we executed a 2D simulation to decrease the computational cost of DEM simulations. The parameters of sand particles and the robot used in the simulations are listed in Table 1. The actual granular materials on asteroid surface are unknown. Hence, we assigned a wide range of particle parameters by referring to Toyoura sand that is used to construct dynamics models of sand particles. The objective of this numerical simulation is to assess the characteristics of this hopping motion qualitatively. Besides, the tendency of the hop angle and the initial velocity against the friction coefficient, the acceleration of gravity, and the angular velocity does not change. For this reason, the size and mass of the robot do not have a significant meaning.

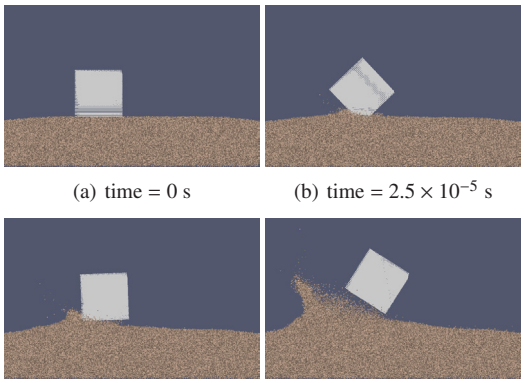

(a) time = 0 s (b) time = 2.5×10^{-5} s

(c) time = 5.0×10^{-5} s (d) time = 1.0×10^{-4} s

Fig. 4. An example of DEM simulation.

4.1. Simulation result

The results of the DEM simulation are discussed in this section. We focused on the hop angle and initial velocity of the robot and analyzed the effects of changing particle parameters.

4.1.1. Hop angle

In this study, the hop angle θ of the robot is defined by the arctangent of the ratio of the horizontal component of the translational velocity to the vertical component of the translational velocity when the corner of the robot begins to detach from the ground surface (as shown in Fig. 5).

$$\theta = \tan^{-1} \frac{v_x}{v_y} \tag{20}$$

In particular, v_x and v_y denote the horizontal and vertical component of the robot's translational velocity.

The results of the hopping simulation are shown in Fig. 6 – Fig. 8. In the figures, μ denotes the friction coefficient of sand particles and μ_r denotes the rolling friction coefficient of sand particles. Furthermore, v_i denotes the velocity required to apply torque to the robot. We analyzed the hop angle of the robot and observed its relation to the acceleration of gravity, friction coefficient of the sand particles, rolling friction coefficient of the sand particles, and torque of the built-in torquer.

- Effect of the Friction Coefficient of Sand Particles
  Initially, the effect of changing friction coefficient of sand particles while the robot was hopping was analyzed. In this simulation, we arrange the other physical parameters listed in Table 2.

Table 1. Robot and particle parameters.

Parameters	Value
Young's Modulus of Sand Particles	5×10^7 N/m
Poisson's Ratio of Sand Particles	0.2
Radius of Sand Particles	6.3×10^{-4} m
Number of Particles	16081
Cohesion of Particles	0 Pa
Size of the Robot	0.05 m cube
Mass of the Robot	1 kg

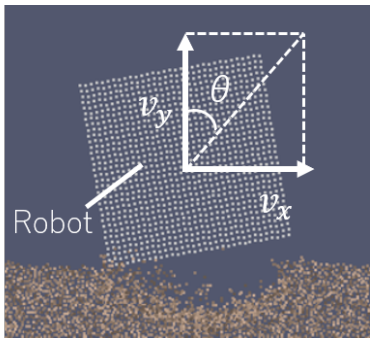

Fig. 5. Definition of hop angle of the robot.

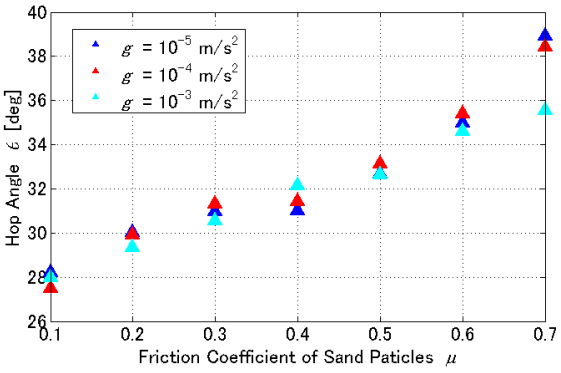

(a) ω = 500 rad/s

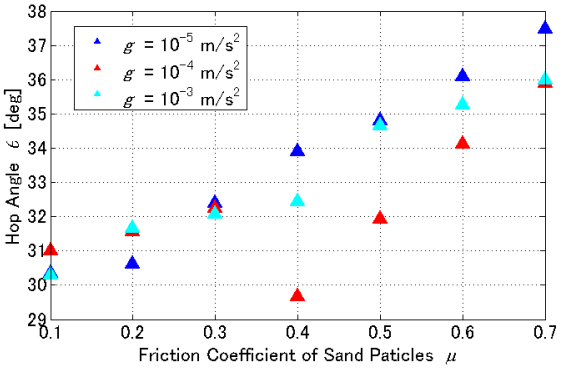

(b) ω = 2000 rad/s

Fig. 6. Hop angle of the robot while changing acceleration of gravity.

As shown in Fig. 6 – Fig. 8, the hop angle of the robot increases when the friction coefficient increases. This is because the horizontal reaction impulses increase when the friction forces (which are derived from the robot touching the sandy surface) increase and finally the horizontal velocity increases.

- Effect of Acceleration of Gravity

  Secondly, the effect of changing the acceleration of gravity while the robot was hopping was analyzed. In this simulation, we assign the other physical parameters listed in Table 3.

Table 2. Parameters for analyzing the effect of μ.

Parameters	Value
g	10^{-5}m/s^2 – 10^{-3}m/s^2
μ	0.1 – 0.7
μ_r	0.1 – 0.3
ω	500 rad/s – 2000 rad/s

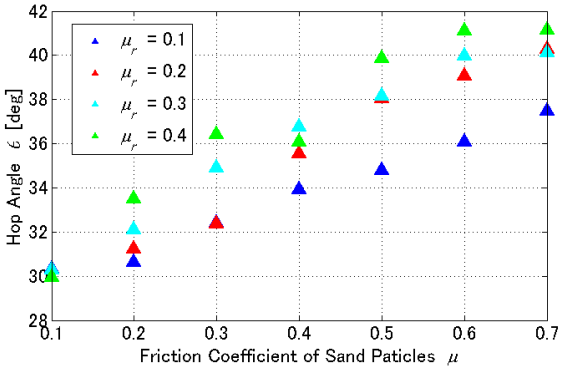

(a) g = 10^{-5} m/s^2

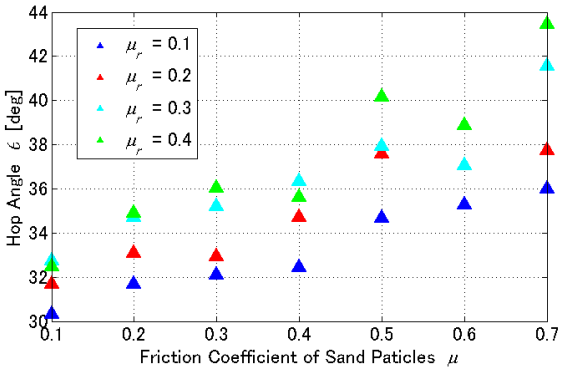

(b) g = 10^{-3} m/s^2

Fig. 7. Hop angle of the robot while changing rolling friction coefficient of sand particles.

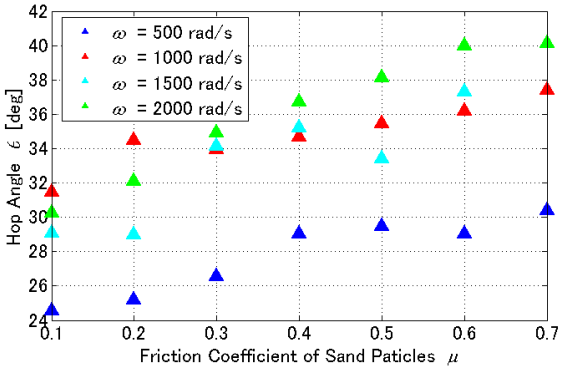

(a) g = 10^{-5} m/s^2

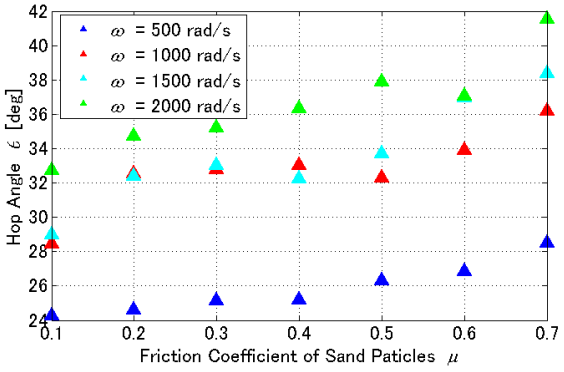

(b) g = 10^{-3} m/s^2

Fig. 8. Hop angle of the robot while changing torque of the torquer.

As shown in Fig. 6, the hop angle of the robot does exhibit a significant change even if the acceleration of gravity changes. This is because the initial velocity is relative to the impulse (which the robot receives from the reaction force), and the impulse depends on the torque of the torquer and not on acceleration of gravity.

- Effect of Rolling Friction Coefficient
  Thirdly, the results of the analysis of the effects of changing the rolling friction coefficient are described. In this simulation, we set the other physical parameters listed in Table 4.
  As shown in Fig. 7, the hop angle of the robot increases when the rolling friction coefficient increases. However, the magnitude was not as high as that while changing the friction coefficient of sand particles. It was observed that most of the hopping motion consists of translational motion, and thus the rolling friction force exhibited a lesser effect when compared with the frictional force.
- Effect of Angular Velocity
  Finally, the effect of changing angular velocity ω was analyzed. In this simulation, we apply the other physical parameters listed in Table 5.
  The hop angle of the robot did not change in the case when the initial angular velocity of the robot corresponded to 1000 rad/s, 1500 rad/s, or 2000 rad/s. Conversely, the hop angle decreased in the case when the initial angular velocity corresponded to 500 rad/s. From generalized Poncelet law, the drag force in granular media is given by the following equation.[16)]

$$D = -f(x) - h(x)\dot{x}^2 \tag{21}$$

From Eq. (21), the drag force D is affected by the position and the velocity of the robot. In particular, D is dominated by the kinetic energy at the higher velocity and the $-h(x)\dot{x}^2$ term in Eq. (21) is not important at the lower velocity. From Fig. 9 and Fig. 10, the velocity of the robot is larger than 1.0 m/s at ω = 700 rad/s and the hop angle θ starts becoming large at ω = 700 rad/s when μ_r is 0.3. When the velocity of the robot is larger than 1.0 m/s, the drag D is dominated by the kinetic energy because of the Eq. (21). This is the reason the magnitude of θ at 1000 rad/s is much larger than that at 500 rad/s.

Specifically, we focused on the relation between the torque of torquer and initial velocity.

Table 3. Parameters for analyzing the effect of g.

Parameters	Value
g	10^{-5}m/s^2 – 10^{-3}m/s^2
μ	0.1 – 0.7
μ_r	0.1
ω	500 rad/s, 2000 rad/s

Table 4. Parameters for analyzing the effect of μ_r.

Parameters	Value
g	10^{-5}m/s^2, 10^{-3}m/s^2
μ	0.1 – 0.7
μ_r	0.1 – 0.3
ω	1500 rad/s

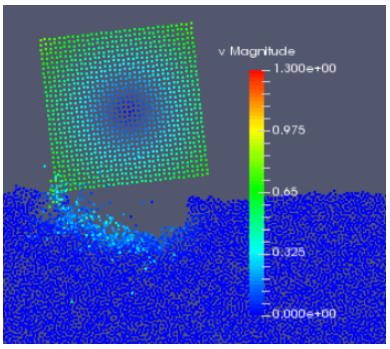

(a) ω = 500 rad/s

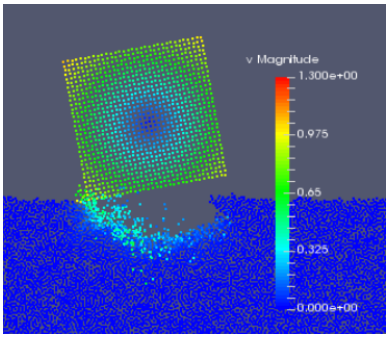

(b) ω = 700 rad/s

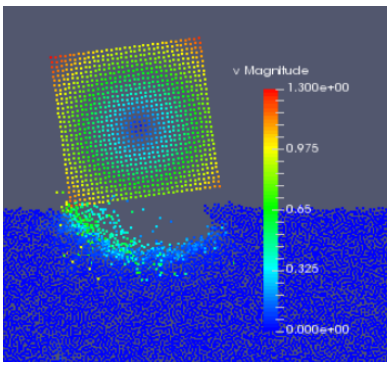

(c) ω = 860 rad/s

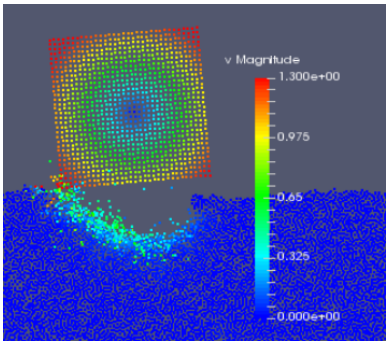

(d) ω = 1000 rad/s

Fig. 9. Velocity of the robot while touching the surface.

4.1.2. Initial velocity of the robot

The results of the simulation are shown in Fig. 11 – Fig. 13. In the figures, μ denotes the friction coefficient of sand

Table 5. Parameters for analyzing the effect of ω.

Parameters	Value
g	10^{-5}m/s^2, 10^{-3}m/s^2
μ	0.1 – 0.7
μ_r	0.1
ω	500 rad/s – 2000 rad/s

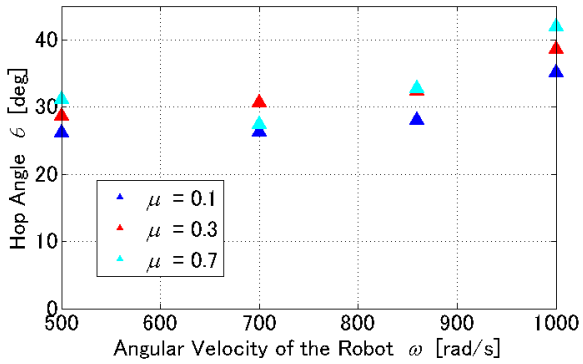

Fig. 10. Relation between ω and θ.

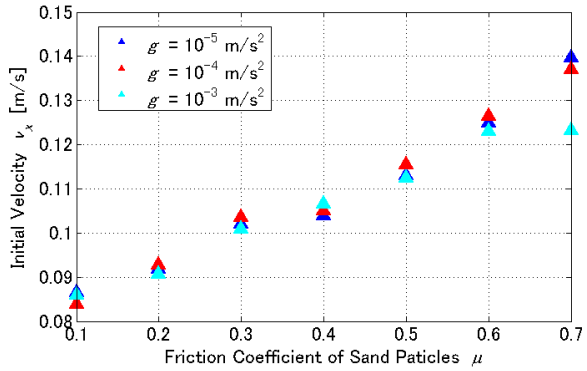

(a) Horizontal Direction

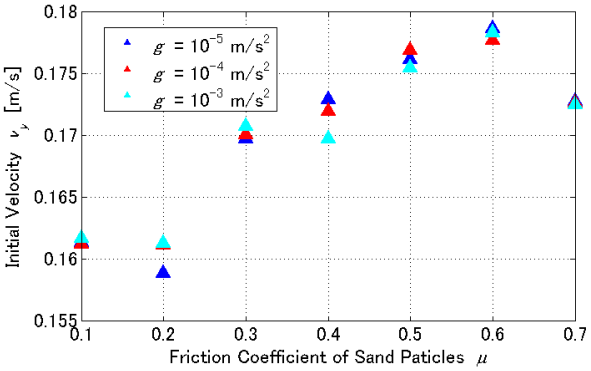

(b) Vertical Direction

Fig. 11. Initial velocity of the robot while changing acceleration of gravity.

particles, and μ_r denotes the rolling friction coefficient of sand particles. Furthermore, v_i denotes the angular velocity required to apply torque to the robot. We analyzed the initial velocity of the robot and compared it while changing the acceleration of gravity, friction coefficient of the sand particles, rolling friction coefficient of sand particles, and torque of the built-in torquer.

- Effect of Friction Coefficient of Sand Particles
  To begin with, the effects of changing friction coefficient are discussed. The physical parameters used in this simulation are listed in Table 2.
  As shown in Fig. 11 – Fig. 13, the horizontal component of the translational velocity increases when the friction coefficient increases. This was because the reaction impulse that the robot received while touching the sandy surface increased. Furthermore, the vertical initial veloc-

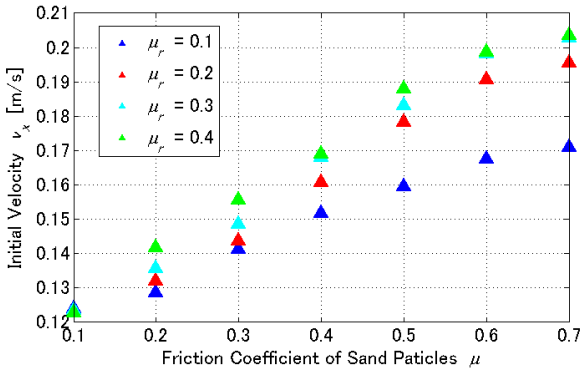

(a) Horizontal Direction

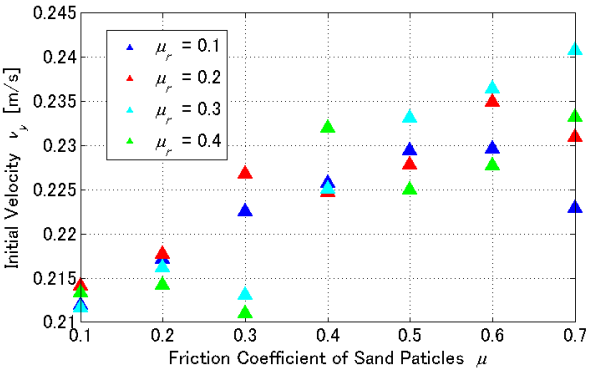

(b) Vertical Direction

Fig. 12. Initial velocity of the robot while changing rolling friction coefficient of sand particles.

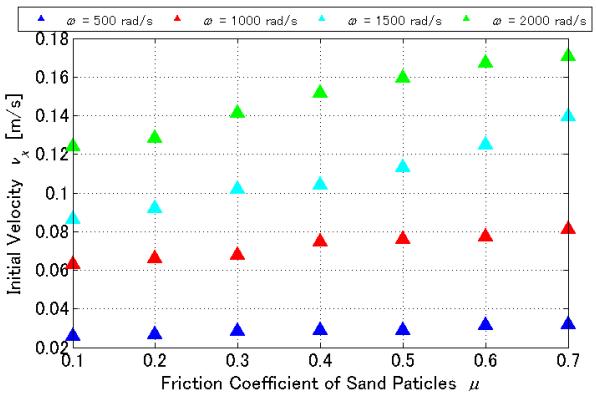

(a) Horizontal Direction

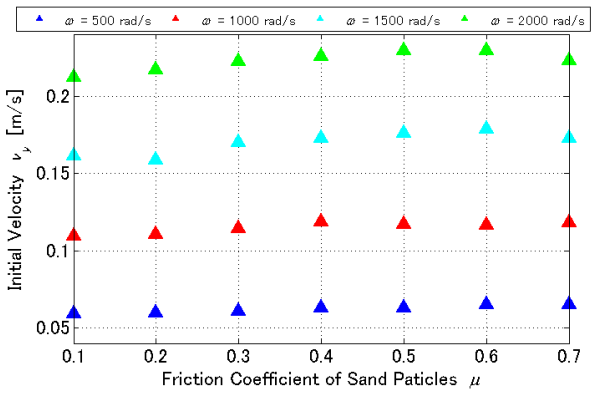

(b) Vertical Direction

Fig. 13. Initial velocity of the robot while changing torque of the torquer.

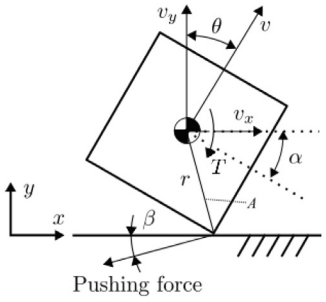

Fig. 14. Dynamics model on the rigid surface.

ity increased. This was because the high friction coefficient lets the ground harden, and thus the robot received a high reaction impulse while hopping.

- Effect of Acceleration of Gravity
  Secondly, we evaluate the effects which g holds. The physical parameters relative to this numerical simulation are listed in Table 3.
  As shown in Fig. 11, the initial velocity did not significantly change when compared with that in the other cases. The impulse which the robot received while touching the surface depends on the friction and rolling friction coefficient of sand particles and the angular velocity of the robot. Therefore, the acceleration of gravity does not affect the motion of the robot before detaching the ground surface.
- Effect of Rolling Friction Coefficient of Sand Particles
  In addition, we address the effects of μ_r which are relative to the hopping motion on a sandy surface. Table 4 shows the physical parameters used in this simulation.
  As shown in Fig. 12, the horizontal component of initial velocity of the robot increases. However, the magnitude of changing initial horizontal velocity was lower than that while changing the friction coefficient. While the robot rotating on the ground surface, the contact point of the robot slips and its motion is translational. Hence, the hopping motion mainly consisted of translational motion. Thus, the rolling friction coefficient affects the motion less than the friction coefficient does.
- Effect of Angular Velocity
  Moreover, we mention the effects of ω which have to do with the hopping motion of the robot. Table 5 exhibits the physical parameters used in this simulation.
  As shown in Fig. 13, the initial velocity of the robot increases as the angular velocity of the robot increases. In Eq. (21), the drag force in granular media D is affected by the position and velocity of the robot. In this case, D becomes large as the angular velocity increases. Thus, the robot receives more impulse while touching the ground surface and obtains more initial hop velocity.

5. Comparison of Hopping Motion on the Sandy Surface and on Rigid Surface

In this section, we compare the hopping motion on the sandy surface with that on the rigid surface.

5.1. Hop angle

We assumed that the case wherein the dynamic friction coefficient of the ground surface was less than 1.0 corresponded to the main case. In this case, the contact point of the robot (see Fig. 14) keeps on slipping on the rigid surface. Therefore, the dynamics model of the robot while touching the surface is given by the following equations:

$$\begin{cases} m\dfrac{d^2x}{dt^2} &= \mu_{d_{\text{ground}}}\dfrac{T}{r}\sin\beta \\ m\dfrac{d^2y}{dt^2} &= \dfrac{T}{r}\sin\beta \end{cases} \tag{22}$$

Specifically, $\mu_{d_{\text{ground}}}$ denotes the dynamic friction coefficient of the ground, T denotes the torque of built-in torque, and r denotes the half length of the diagonal of the robot. From the motion equations, the ratio of initial velocity v_x/v_y is equal to the dynamic friction coefficient of the ground surface, and this leads to the following equation:

$$\theta = \tan^{-1}\frac{v_x}{v_y} = \tan^{-1}\mu_{d_{\text{ground}}} < 45^\circ \tag{23}$$

Conversely, when the robot hops on the granular surface, the hop angle of the robot is as shown in Fig. 7 – Fig. 5. As shown in the figures, the hop angle significantly exceeds that in the case of the robot hopping on the rigid surface when the friction coefficient is low. However, the hop angle was almost equal to that in the case of the robot hopping on the rigid surface when the friction coefficient approached 0.9. When the friction coefficient was near 0.1, the sandy surface was soft. Therefore, the robot moved into the soft surface and received the drag force described in Eq. (21) in addition to the frictional force, and thus the ratio of impulse which the robot received while touching the ground became large. Conversely, when the friction coefficient was near 0.9, the sandy surface became hard. Therefore, the characteristics of the sandy surface resembled that of a rigid surface, and thus the robot received a relatively low impulse while touching the ground. Thus, the results of hop angle are as stated above.

5.2. Initial velocity

Based on Eq. (22), we analyze the result of numerical simulation. The simulation conditions are listed in Table 6. Figure 15 shows the initial horizontal velocity of the robot while hopping on the rigid surface. In this simulation, the angular velocity for rotating robot was 2000 rad/s for comparing the hopping motion on sandy surface with that on rigid surface. A comparison of Fig. 11 with Fig. 15 indicates that the initial velocity of the robot while hopping on the sandy surface is lower than that on the rigid surface. This is because the robot received less impulse while touching the surface due to the soft sandy surface. However, even on the sandy surface, the initial translational velocity of the robot increased when the friction coefficient of sand particles approached 0.9, and the value was almost equal to that

Table 6. Conditions of the hopping simulation on the rigid surface.

Parameters	Value
g	10^{-5}m/s^2
$\mu_{d_{\text{ground}}}$	0.1 – 0.7
Size of the Robot	0.05 m cube
Mass of the Robot	1 kg

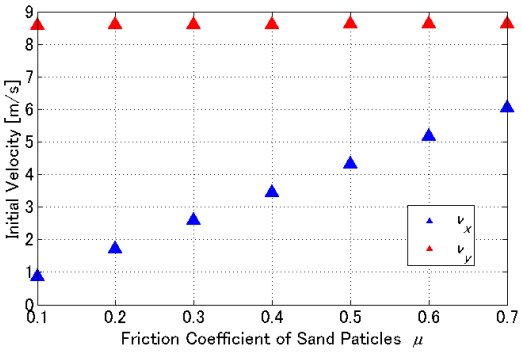

Fig. 15. Initial velocity of the robot on the rigid surface.

while hopping on the rigid surface. This was because the robot received higher reaction impulse while touching the surface because the sandy surface became hard when the friction coefficient of sand particles increased.

6. Conclusion

In the study, the hopping motion of the robot on sandy surface was analyzed by using DEM. We focused on the hop angle and initial hop velocity of the robot and compared the hopping motion on a sandy surface and rigid surface. The results indicated that the hop angle and initial hop velocity increase when the friction coefficient, rolling friction coefficient of sand particles increase. Moreover, the results indicated that the drag force which the robot receives follows generalized Poncelet law while the robot touching the surface. Conversely, the hop angle and initial hop velocity were not affected by acceleration of gravity. This leads that it is especially important to apply large torque to the robot in order to obtain large traveling distance at each hop on sandy surface. Furthermore, the controllability of the hopping motion was proved due to the results that the hop angle and initial velocity increase when the torque of the torquer increase. A comparison of the hopping motion on the two surfaces indicated the hop angle of the robot while hopping on the sandy surface exceeded that on the rigid surface. Conversely, the initial velocity of the robot while hopping on the sandy surfaces decreased although the robot obtained sufficient initial velocity to hop and hopping motion was also feasible on sandy surfaces. For the future missions, we have to automate the robot and make the navigation algorithm by using the analysis results.

References

1) Kawaguchi, J., Uesugi, T., Fujiwara, A., and Saito, H.: The MUSES-C, Mission Description and Its Status, *Acta Astronautica*, **45** (1999), pp. 397–405.
2) Wittmann, K., Feuerbacher, B., Ulamec, S., Rosenbauer, H., Bibring, J., P., Moura, D., Mugnuolo, R., diPippo, S., Szego, K., and Haerendel, G.: Rosetta lander in Situ Characterization of a Comet Nucleus, *Acta Astronautica*, **45** (1999), pp. 389–395.
3) Yano, H., Kubota, T., Miyamoto, H., Okada, T., Scheeres, D., Takagi, Y., Yoshida, K., Abe, M., Abe, S., Barnouin-Jha, O., Fujiwara, A., Hasegawa, S., Hashimoto, T., Ishiguro, M., Kato, M., Kawaguchi, J., Mukai, T., Saito, J., Sasaki, S., and Yoshikawa, M.: Touchdown of the Hayabusa Spacecraft at the Muses Sea on Itokawa, *Science*, **312** (2006), pp. 1350–1353.
4) Kawaguchi, J., Fujiwara, A., and Uesugi, T.: Hayabusa-Its Technology and Science Accomplishment Summary and Hayabusa-2, *Acta Astronautica*, **62** (2008), pp. 639–647.
5) Wilcox, B., H. and Jones, R., M.: The MUSES-CN Nanorover Mission and Related Technology, The 2000 IEEE Aerospace Conference, Big Sky, United States, pp. 639–647, 2000.
6) Yoshimitsu, T., Kubota, T., Nakatani, I., Adachi, T., and Saito, H.: Micro-hopping Robot for Asteroid Exploration, *Acta Astronautica*, **52** (2003), pp. 441–446.
7) Witte, L., Biele, J., Braukhane, A., Herrman, F., Ho, T. M., Krause, C., Kuß, S., Lange, C., Schotterer, M., Ulamec, S., and Wagenbach, S.: The Mobile Asteroid Surface Scout(MASCOT) - System & Mission Engineering and Surface Operations Concept, Global Space Exploration Conference, Washington D.C., United States, GLEX-2012,06,2,6,x12650, 2012.
8) Hockman, B., Frick, A., Reid, R., G., Nesnas, I., A., D., and Pavone, M.: Design, Control, and Experimentation of Internally-Actuated Rovers for the Exploration of Low-gravity Planetary Bodies, *J. Field Robotics*, **34** (2017), pp. 5–24.
9) Miyamoto, H., Yano, H., Scheeres, D., J., Abe, S., Barnouin-Jha, O., Cheng, A., F., Demura, H., Gaskell, R., W., Hirata, N., Ishiguro, M., Michikami, T., Nakamura, A., M., Nakamura, R., Saito, J., and Sasaki, S.: Regolith Migration and Sorting on Asteroid Itokawa, *Science*, **316** (2007), pp. 1011–1014.
10) Nakashima, H., Fujii, H., Oida, A., Momozu, M., Kanamori, H., Aoki, S., Yokoyama, T., Shimizu, H., Miyasaka, J., and Ohdoi, K.: Discrete Element Method Analysis of Single Wheel Performance for a Small Lunar Rover on Sloped Terrain, *J. Terramechanics*, **47** (2010), pp. 307–321.
11) Ebert, T. and Larochelle, P.: Simulation Soft Regolith Dynamic Anchors for Celestial Exploration, The 2016 IEEE Aerospace Conference, Big Sky, United States, 2016.
12) Cundall, P., A. and Strack, O. D. L.: A Discrete Numerical Model for Granular Assemblies, *Geotechnique*, **29** (1979), pp. 47–65.
13) Renzo, A., D. and Maio, F., P., D.: Comparison of Contact-force Models for the Simulation of Collisions in DEM-based Granular Flow Codes, *Chemical Engineering Science*, **59** (2004), pp. 525–541.
14) Renzo, A., D. and Maio, F., P., D.: An Improved Integral Non-linear Model for the Contact of Particles in Distinct Element Simulations, *Chemical Engineering Science*, **60** (2005), pp. 1303–1312.
15) Ai, J., Chen, J.-F., Rotter, M., J., and Ooi, Y. J.: Assessment of Rolling Resistance Models in Discrete Element Simulations, *Powder Technology*, **206** (2011), pp. 269–282.
16) Tiwari, M., Mohan, K., R., T., and Sen, S.: Drag-force Regimes in Granular Impact, *Physical Review E*, **90** (2014), 062202.